Angular distribution of the dielectronic satellite lines from relativistic high-Z ions: Multipole-mixing effects

Stephan Fritzsche*
Gesellschaft für Schwerionenforschung (GSI), D-64291 Darmstadt, Germany
and Max-Planck-Institut für Kernphysik, Saupfercheckweg 1, D-69117 Heidelberg, Germany

Nikolay M. Kabachnik
Gesellschaft für Schwerionenforschung (GSI), D-64291 Darmstadt, Germany
and Institute of Nuclear Physics, Moscow State University, Moscow 119991, Russia

Andrey Surzhykov
Physikalisches Institut, Universität Heidelberg, D-69120 Heidelberg, Germany
(Received 11 June 2008; published 8 September 2008)

The dielectronic recombination of high-Z hydrogenlike ions is studied within the framework of the density matrix theory. Emphasis is placed on the alignment of the doubly excited ions and the non-electric-dipole ($E1$) contributions to the subsequent characteristic x-ray emission. Multiconfiguration Dirac-Fock calculations have been carried out in order to investigate the multipole mixing effects on the radiative decay of the doubly excited resonances of heliumlike uranium, following the K-LL dielectronic recombination of hydrogenlike U^{91+} ions. In particular, the angular distribution of the $K\alpha_1$ hypersatellites is notably modified by the interference between the leading $E1$ and the magnetic-quadrupole ($M2$) transitions. The results are compared with measurements and previous computations available.

DOI: 10.1103/PhysRevA.78.032703 PACS number(s): 34.80.Lx, 31.15.A−, 31.30.J−, 34.70.+e

I. INTRODUCTION

Dielectronic recombination (DR) is a resonant process in which a free electron is captured into an ion under the simultaneous excitation of one or several bound electrons, and where the multiply excited ion is stabilized afterwards by photon emission. During the last decades, this resonant capture process has found considerable interest, both by experiment and theory, because it occurs frequently in astrophysical and laboratory plasmas [1–3]. However, DR plays an important role also in studying the electronic and hyperfine structure of ions [4] as well as the relativistic effects on the electron-electron interaction in high-Z ions [5,6]. Therefore, a large number of DR experiments have been carried out at storage rings and electron-beam ion traps during recent years (see Ref. [7] for a detailed discussion and further references).

While experiments with mid- and high-Z elements have been carried out at electron coolers of various storage rings worldwide and provided us with a great deal of high-precision data on the level structure and resonance strengthes of doubly and inner-shell excited ions [7–9], carbon [10,11] and gas-jet targets [12] were employed in studying the angular distribution of the characteristic x-ray emission following the DR or radiative capture of electrons by fast projectiles [13,14]. In all these ion-electron or ion-atom collisions, the ion beam presents a preferred direction for the collision system and, hence, provides conditions for an alignment of the multiply excited ions, i.e., an unequal population of the ionic sublevels with different modulus $|M_J|$ of the magnetic quantum number. In the subsequent radiative stabilization of the ions, this alignment is partially transferred to the lower-lying levels of the recombined ion and also affects the emitted radiation, leading in many cases to an anisotropic angular distribution and linear polarization of the characteristic photons [15–17]. From the detailed analysis of these photons, therefore, valuable information can be obtained about the capture process and the magnetic sublevel population of the doubly excited states.

For the DR of high-Z ions, the angular distribution of the characteristic x-ray emission has been studied at the ESR storage ring in Darmstadt [12]. In these experiments, hydrogenlike U^{91+} projectiles were scattered by a molecular H_2 target in order to form the doubly excited LL resonances of the heliumlike ions. Instead of a free electron, hereby a weakly bound (quasifree) target electron with a given momentum distribution (Compton profile) was captured, a process that is known from the literature also as resonant transfer and excitation (RTE). Owing to the large projectile energy of about 100 MeV/u, that is needed to form the K-LL resonances with heavy hydrogenlike ions, the Compton profile of the H_2 target electrons is not so important, and the RTE and DR processes result practically in the same photon spectra. For the capture into high-Z hydrogenlike ions, moreover, the doubly excited LL resonances stabilize predominantly via the subsequent emission of two $K\alpha$ photons which are often referred to as the hypersatellite (HS) and satellite photons [18]. In the experiments by Ma and co-workers [12], the angular distributions of the $K\alpha_{1,2}$ lines have been measured and compared with theoretical predictions [19,20]. Although a reasonable agreement between experiment and theory was found for most groups of lines, a rather remarkable discrepancy remained for the angular distribution of the $K\alpha_1$ HS lines that arise from the decay of the $L_{1/2}L_{3/2}$ reso-

*s.fritzsche@gsi.de

nances. For this line group, the theoretically predicted anisotropy of the $K\alpha_1$ HS underestimates the observations by more than a factor of 2 [12,19], a discrepancy that has not been resolved until now.

In all previous theoretical investigations, however, only the electric-dipole ($E1$) radiation has been taken into account in analyzing the angular distribution of the $K\alpha_1$ HS lines. As pointed out already in Ref. [12], a rather strong anisotropy of some of the lines could be caused also by higher multipoles in the expansion of the electron-photon interaction, and especially by their interference with the $E1$ radiation. Such strong interference effects between the $E1$ and $M2$ (magnetic quadrupole) transitions have been found recently for the Ly-α decay of hydrogenlike uranium, following the radiative electron capture (REC) into the $2p_{3/2}$ level of initially bare ions [21]. For the Ly-α_1 radiation, this multipole mixing increased the calculated anisotropy by almost 30%, in very good agreement with experiment [13]. Therefore, a similar effect of the multipole mixing can be expected also for the characteristic emission from few-electron ions. In the present work, we apply the density matrix theory to describe the $K\alpha$ HS radiation of high-Z, heliumlike ions, following the DR into initially hydrogenlike ions. Combined with the multiconfiguration Dirac-Fock method, this treatment enables us to account for the dominant relativistic, many-body and multipole-mixing effects consistently within the same framework.

In the next section, we provide the basic formulas to describe the DR of few-electron ions as a two-step process that includes (i) the resonant capture and (ii) the subsequent radiative stabilization. In particular, here we discuss the statistical tensors of the doubly excited resonances which help characterize their magnetic sublevel population (Sec. II A). The relation between these tensors and the angular distribution of the subsequent radiation is discussed in Sec. II B, keeping the formalism general enough to deal with different (many-electron) configurations of the ions. Apart from the alignment of the doubly excited resonances, however, the angular distribution depends also on the so-called structure function that accounts for the multipole-mixing effects in the course of the radiative stabilization. All computations, as briefly summarized in Sec. III, are based on either the multiconfiguration Dirac-Fock (MCDF) method or an independent-particle model (IPM). The latter model has been utilized to explore some basic features of the structure function. In Sec. IV detailed computations are presented for various nuclear charges, $2 \leqslant Z \leqslant 92$, but with emphasis on the angular distribution of the $K\alpha_1$ HS line following the DR into the $L_{1/2}L_{3/2}$ resonances of initially hydrogenlike U^{91+} ions. For these ions, the multipole-mixing effects are found to enhance the anisotropy of this line by about 30%. Finally, a brief summary of our results and their implication for forthcoming angle-resolved DR studies are given in Sec. V.

II. THEORY

To describe the DR of few-electron ions, we consider the two-step process

$$A^{n+}(\alpha_0 J_0) + e^-(\epsilon lj) \rightarrow A^{(n-1)+**}(\alpha_d J_d) \rightarrow A^{(n-1)+*}(\alpha_f J_f) + \gamma, \tag{1}$$

where the first step is the resonant capture of an electron with energy ϵ, total angular momentum j, and orbital angular momentum l into the ion A^{n+}, and the second step is given by its radiative stabilization. In the notation (1), the ion is supposed to be initially n-times ionized and in a state $|\alpha_0 J_0\rangle$ with well-defined total angular momentum J_0. When the electron is captured, the ion charge is reduced by one, and the resonance state $|\alpha_d J_d\rangle$ is formed which decays by the emission of a photon γ into one of the final states $|\alpha_f J_f\rangle$. In Eq. (1), α_0, α_d, and α_f hereby denote all of the additional quantum numbers that are needed to describe the ionic states uniquely. Typically, the final state $|\alpha_f J_f\rangle$ of the DR process (1) will decay further by photon emission until the ground state of the ion is reached; especially in the K-LL dielectronic recombination of hydrogenlike ions, the first emitted photon is a HS photon while the second photon is a satellite photon [18]. In the present work, we shall restrict ourselves to the angular distribution of the first HS photon for which the analysis and comparison with experiment is much simpler than for the subsequent satellite emission because the $|\alpha_d J_d\rangle$ doubly excited states are populated only by the K-LL DR process. In contrast, the satellites may arise also from excitation and REC processes, including possible cascades [12]. These additional processes aggravate the analysis for the satellites and often requires to average over the photon distributions from different decay mechanisms.

A. Dielectronic recombination cross sections and alignment parameters

To describe the process (1) quantum mechanically, it is convenient to utilize the density matrix theory [16,22] and to express the DR cross sections and alignment of the intermediate doubly excited states in terms of their statistical tensors, $\rho_{k0}(\alpha_d J_d)$ with rank k and its projection $q=0$ upon the quantization axis [23,24]. Using the standard techniques for the recoupling of angular momenta, the evaluation of these tensors can be traced back to the reduced amplitudes $\langle \alpha_d J_d \| V \| \alpha_0 J_0, lj:J_d \rangle$ which describe the formation of the resonance $|\alpha_d J_d\rangle$ due to the electron-electron (e-e) interaction between the bound electrons in the initial state $|\alpha_0 J_0\rangle$ and the free electron (lj). This reduced matrix element for the resonant capture of an electron coincides, up to a phase factor, with the amplitude for the time-reversed process of the Auger decay. Following Ref. [24] (Sec. 2.1.2), the statistical tensors of the resonance can be written as

$$\begin{aligned}\rho_{k0}(\alpha_d J_d) = & \frac{c}{8\pi(2J_0+1)} \sum_{ll'jj'} (-1)^{J_d+J_0-1/2} \\ & \times [l,l',j,j']^{1/2} \langle l0l'0|k0\rangle \begin{Bmatrix} j & l & 1/2 \\ l' & j' & k \end{Bmatrix} \\ & \times \begin{Bmatrix} j & J_d & J_0 \\ J_d & j' & k \end{Bmatrix} \langle \alpha_d J_d \| V \| \alpha_0 J_0, lj:J_d \rangle \\ & \times \langle \alpha_d J_d \| V \| \alpha_0 J_0, l'j':J_d \rangle^*, \end{aligned} \tag{2}$$

where the z axis (quantization axis) is chosen along the direction of the beam, and where it is supposed that neither the ion nor the electron are initially polarized. In expression (2), moreover, c is a normalization constant, $\langle l0l'0|k0\rangle$ a Clebsch-Gordan coefficient, $[a,b,\ldots]\equiv(2a+1)(2b+1)\ldots$, and the standard notation for the Wigner $6j$ symbols has been utilized.

In practice, it is convenient to choose the normalization constant in Eq. (2) in such a way that the zero-rank statistical tensor is proportional to the DR capture rate, $[J_d]^{1/2}\rho_{00}(\alpha_d J_d)=P_{cap}(0\to d)$; with this convention in mind, we find $c=8\pi^2$ and

$$P_{\mathrm{cap}}(0\to d)=\frac{2\pi}{2(2J_0+1)}\sum_{lj}|\langle\alpha_d J_d\|V\|\alpha_0 J_0,lj{:}J_d\rangle|^2$$

$$=\frac{(2J_d+1)}{2(2J_0+1)}P_A(d\to 0), \tag{3}$$

where $P_A(d\to 0)$ denotes the corresponding Auger rate for the time-reversed transition [16]. The DR capture rate determines the initial population of the doubly excited states and, thus, affects also the intensity of the corresponding (hyper) satellite lines in the photon spectra.

It is often more appropriate to describe the sublevel population of the excited ions in terms of the reduced statistical tensors or the so-called alignment parameters $\mathcal{A}_{k0}(\alpha_d J_d)=\rho_{k0}(\alpha_d J_d)/\rho_{00}(\alpha_d J_d)$, which define the angular distribution and polarization of the subsequent photon emission [24,25]. Making use of Eq. (2), the alignment parameters of the excited ion can be expressed as

$$\mathcal{A}_{k0}(\alpha_d J_d)=N^{-1}[J_d]^{1/2}\sum_{ll'jj'}(-1)^{J_d+J_0-1/2}$$
$$\times[l,l',j,j']^{1/2}\langle l0l'0|k0\rangle\begin{Bmatrix} j & l & 1/2\\ l' & j' & k\end{Bmatrix}$$
$$\times\begin{Bmatrix} j & J_d & J_0\\ J_d & j' & k\end{Bmatrix}\langle\alpha_d J_d\|V\|\alpha_0 J_0,lj{:}J_d\rangle$$
$$\times\langle\alpha_d J_d\|V\|\alpha_0 J_0,l'j'{:}J_d\rangle^*, \tag{4}$$

with $N=\Sigma_{lj}|\langle\alpha_d J_d\|V\|\alpha_0 J_0,lj{:}J_d\rangle|^2$, and by including a summation over all partial waves (lj) of the free electron that fulfill the angular-momentum coupling condition, $\delta(J_0,j,J_d)=1$.

For an aligned ion, the tensor $\mathcal{A}_{k0}(\alpha_d J_d)$ is nonzero only if the rank k is even and $k\leqslant 2J_d$. Therefore, the magnetic sublevel population of the doubly excited states with $J_d=1$ can be described by the single parameter $\mathcal{A}_{20}(\alpha_d J_d=1)$, while two parameters $\mathcal{A}_{20}(\alpha_d J_d=2)$ and $\mathcal{A}_{40}(\alpha_d J_d=2)$ are needed for the case of $J_d=2$.

B. Angular distribution of the subsequent radiative decay

Owing to the alignment of the excited ion, the subsequent photon emission is in general anisotropic and linearly polarized. In fact, the angular and polarization properties of the emitted photons are closely related to the alignment parameters $\mathcal{A}_{k0}$. For example, the angular distribution of the HS photons in the second step of the DR process (1), $|\alpha_d J_d\rangle\to|\alpha_f J_f\rangle+\gamma^{HS}$, is given by [25,26]

$$W^{\mathrm{dec}}(\theta)=\frac{\Gamma_{df}}{4\pi}\left(1+\sum_{k=2,4,\ldots}\beta_k P_k(\cos\vartheta)\right), \tag{5}$$

where

$$\beta_k\equiv\beta_k(\alpha_d J_d,\alpha_f J_f)=f_k(\alpha_d J_d,\alpha_f J_f)\mathcal{A}_{k0}(\alpha_d J_d) \tag{6}$$

denotes the anisotropy parameter, $\Gamma_{df}\equiv\Gamma_{\alpha_d J_d\to\alpha_f J_f}$ the decay rate of this HS transition, $P_k(\cos\vartheta)$ is the Legendre polynomial, and the angle ϑ refers to the propagation direction of the emitted photons with regard to the ion beam.

Apart from the reduced statistical tensors $\mathcal{A}_{k0}(\alpha_d J_d)$, the photon angular distribution also depends on the so-called structure functions $f_k(\alpha_d J_d,\alpha_f J_f)$ of the HS transition, as seen from Eq. (6). These structure functions merely reflect the electronic structure of the ion and characterize a given radiative transition. They are independent of how the initial resonance was created, i.e., independent of the resonant electron capture in the present case. These functions contain the matrix elements of different multipole components, that arise from the expansion of the electron-photon interaction operator and that are allowed for a given transition. Following Ref. [26], the structure function of rank k is given by

$$f_k(\alpha_d J_d,\alpha_f J_f)=\frac{\sqrt{2J_d+1}}{2}\sum_{LpL'p'}i^{L'+p'-L-p}$$
$$\times(-1)^{J_f+J_d+k+1}[L,L']^{1/2}\langle L1L'-1|k0\rangle$$
$$\times(1+(-1)^{L+p+L'+p'-k})\begin{Bmatrix} L & L' & k\\ J_d & J_d & J_f\end{Bmatrix}$$
$$\times\langle\alpha_d J_d\|H_\gamma(pL)\|\alpha_f J_f\rangle\langle\alpha_d J_d\|H_\gamma(p'L')\|\alpha_f J_f\rangle^*$$
$$\times\left(\sum_{Lp}|\langle\alpha_d J_d\|H_\gamma(pL)\|\alpha_f J_f\rangle|^2\right)^{-1}, \tag{7}$$

where $\langle\alpha_d J_d\|H_\gamma(pL)\|\alpha_f J_f\rangle$ denotes the reduced matrix element for the multipole transition (pL). In this notation, $p=0$ refers to the magnetic and $p=1$ to the electric multipoles of order L [27,28]. Equations (5)–(7) represent the most general form of the angular distribution of the characteristic radiation following the resonant electron capture of unpolarized electrons by an unpolarized ion beam; they include the summation over all the multipoles (pL) of the radiation field that are allowed owing to the parity and angular-momentum selection rules.

Equations (5) and (7) simplify considerably if only one multipole component is allowed for a given initial and final state. For the—often dominant—electric-dipole $(E1)$ emission, for example, the angular distribution is given by the well-known formula [24,25]

$$W^{\mathrm{dec}}_{E1}(\theta)=\frac{\Gamma_{df}}{4\pi}[1+f_2(\alpha_d J_d,\alpha_f J_f;E1)\mathcal{A}_{20}(\alpha_d J_d)P_2(\cos\vartheta)], \tag{8}$$

where the structure function

$$f_2(\alpha_d J_d, \alpha_f J_f; E1) = (-1)^{1+J_d+J_f} \sqrt{\frac{3(2J_d+1)}{2}} \begin{Bmatrix} 1 & 1 & 2 \\ J_d & J_d & J_f \end{Bmatrix} \tag{9}$$

coincides in this case with the anisotropy parameter $\alpha_2^{\rm ph}$ of Refs. [25,24]: $f_2(\alpha_d J_d, \alpha_f J_f; E1) \equiv \alpha_2^{\rm ph}$. For a pure electric-dipole emission, obviously, the structure function does not depend on the amplitude of the bound-bound transition and, hence, reduces to a geometrical factor that is independent of the nuclear charge Z for any transition along some given isoelectronic sequence.

Finally, let us note that the angular distributions (5) and (8) are written in the rest frame of the ion. For the DR into a fast-moving heavy ion, these distributions should be transformed into the laboratory frame in order to become comparable with observations. This transformation often leads to an asymmetry of the angular emission pattern with respect to the plane perpendicular to the beam.

III. COMPUTATIONS

For the further analysis of the statistical tensors of the doubly excited states and for studying the angular distribution of the subsequent photon emission, we need to calculate the reduced matrix elements $\langle \alpha_d J_d \| V \| \alpha_0 J_0, lj:J_d \rangle$ and $\langle \alpha_d J_d \| H_\gamma(pL) \| \alpha_f J_f \rangle$ for the resonant electron capture and the multipole transitions, respectively. Since these matrix elements occur frequently in the computation of a large variety of atomic properties [27,29,30], they have been considered in many different approximations. For highly charged ions especially, the multiconfiguration Dirac-Fock (MCDF) method has been found a versatile tool to account for the relativistic and many-body effects on the same footings, while the independent-particle model (IPM) allows for a simplification in the formalism that often gives rise to a better insight into the underlying mechanisms.

A. Multiconfiguration Dirac-Fock approach

The MCDF method has been described in detail in the literature [31–33]. In this method, an atomic state wave function is approximated by a linear combination of configuration state functions (CSFs) of the same symmetry

$$\psi_\alpha(PJM) = \sum_{r=1}^{n_c} c_r(\alpha) | \gamma_r PJM \rangle, \tag{10}$$

where n_c is the number of CSFs and $\{c_r(\alpha)\}$ denotes the representation of the atomic state in this basis. In most standard computations, the CSFs $|\gamma_r PJM\rangle$ are constructed as antisymmetrized products of a common set of orthonormal orbitals and are optimized together on the basis of the Dirac-Coulomb Hamiltonian. Relativistic effects due to the Breit interaction are then added to the representation $\{c_r(\alpha)\}$ by diagonalizing the Dirac-Coulomb-Breit Hamiltonian matrix [34,35]. The dominant QED corrections due to the self-energy of the bound electrons and the polarization of the vacuum were also estimated. They shift the level energies but do not affect the wave functions in the computation of the transition amplitudes for the resonant electron capture and the multipole transitions. For these computations, we used the ANCO [36], AUGER [37] and REOS [29] components which have been developed within the framework of the RATIP program [33,38]. For the amplitudes $\langle \alpha_d J_d \| V \| \alpha_0 J_0, lj:J_d \rangle$ of the resonant electron capture, moreover, both the Coulumb as well as the Breit interaction, $V = V_{\rm Coulomb} + V_{\rm Breit}$ were taken into account in order to obtain a proper relative population of the LL resonances [39].

B. Independent-particle model with hydrogenic orbitals

While the proper treatment of the e-e interaction is essential for the resonant capture of an electron, i.e., the first step of the DR process (1), correlation effects play only a minor role in the second step, the radiative stabilization of high-Z, heliumlike ions. Therefore, in order to provide better insight into the mixing of different multipole transition, we calculated the structure functions (7) of the HS transition not only within the MCDF but also the IPM model in which the wave function of the atomic states is represented by a single Slater determinant, built from hydrogenic orbitals. In this simple model, the amplitudes for the multipole transitions can be easily expressed in terms of the single-particles amplitudes for the active electron, a reduction that reads for a two-electron system as [40,41]

$$\begin{aligned} \langle \alpha_d J_d \| H_\gamma(pL) \| \alpha_f J_f \rangle &= \langle (n_s j_s, n_d j_d) J_d \| H_\gamma(pL) \| (n_s j_s, n_f j_f) J_f \rangle \\ &= (-1)^{j_f - J_d + L + j_s} \begin{Bmatrix} j_s & j_f & J_f \\ L & J_d & j_d \end{Bmatrix} \\ &\quad \times [J_d, J_f]^{1/2} \langle n_d j_d \| H_\gamma(pL) \| n_f j_f \rangle, \end{aligned} \tag{11}$$

and where the second electron is assumed to be kept frozen during the radiative stabilization.

Equation (11) has been utilized to compute the structure function in the effective one-particle model [42]. In these computations, the nuclear screening effect was taken into account by adjusting the nuclear charge $Z_{\rm eff}$ so that the correct $|\alpha_d J_d\rangle \to |\alpha_f J_f\rangle$ transition energy was obtained. When compared with the MCDF calculations from Sec. III A, the structure function from the IPM model agrees within about 2% along the whole helium isoelectronic sequence, except for the singlet-triplet intercombination transitions at the low-Z end of the isoelectronic sequence which require a proper superposition of the $J=1$ configuration states. Such a linear combination of different symmetry-adapted CSFs cannot be accounted for in the IPM model.

IV. RESULTS AND DISCUSSION

A. Anisotropy of the fine-structure components of the $K\alpha_{1,2}$ hypersatellite lines

We focus on the question of how the multipole mixing affects the angular distribution of $K\alpha$ radiation from aligned heavy ions. For hydrogenlike high-Z projectiles, the K-LL DR leads to 10 doubly excited $|2lj, 2l'j'(J)\rangle$ resonances (briefly referred to as LL resonances), cf. Table I. From these 10 resonance levels, six have a total angular momentum $J_d > 0$ and, hence, can give rise to an anisotropic photon emis-

TABLE I. Hypersatellite transitions from the *LL* resonances of heliumlike ions. Beside the initial and final state dominant configurations of the transitions, their classification into $K\alpha_1$ ($2p_{3/2} \rightarrow 2s_{1/2}$) and $K\alpha_2$ ($2p_{1/2} \rightarrow 2s_{1/2}$) lines as well as the allowed multipole components are listed.

Resonance group	Doubly excited initial state	Transition	Singly excited final state	Allowed multipoles
$L_{1/2}L_{1/2}$	$2s_{1/2}2p_{1/2}$ $(J=0)$	$K\alpha_2$	$1s_{1/2}2s_{1/2}$ $(J=1)$	$E1$
		$K\alpha_2$	$1s_{1/2}2p_{1/2}$ $(J=1)$	$M1$
$L_{1/2}L_{1/2}$	$2s_{1/2}2s_{1/2}$ $(J=0)$	$K\alpha_2$	$1s_{1/2}2s_{1/2}$ $(J=1)$	$M1$
$L_{1/2}L_{1/2}$	$2s_{1/2}2p_{1/2}$ $(J=1)$	$K\alpha_2$	$1s_{1/2}2s_{1/2}$ $(J=1)$	$E1$, $M2$
		$K\alpha_2$	$1s_{1/2}2p_{1/2}$ $(J=1)$	$M1$, $E2$
		$K\alpha_2$	$1s_{1/2}2s_{1/2}$ $(J=2)$	$E1$, $M2$, $E3$
		$K\alpha_2$	$1s_{1/2}2p_{1/2}$ $(J=0)$	$M1$
$L_{1/2}L_{1/2}$	$2p_{1/2}2p_{1/2}$ $(J=0)$	$K\alpha_2$	$1s_{1/2}2p_{1/2}$ $(J=1)$	$E1$
$L_{1/2}L_{3/2}$	$2s_{1/2}2p_{3/2}$ $(J=2)$	$K\alpha_1$	$1s_{1/2}2s_{1/2}$ $(J=1)$	$E1$, $M2$, $E3$
		$K\alpha_1$	$1s_{1/2}2s_{1/2}$ $(J=0)$	$M2$
		$K\alpha_2$	$1s_{1/2}2p_{3/2}$ $(J=2)$	$M1$, $E2$, $M3$, $E4$
		$K\alpha_2$	$1s_{1/2}2p_{3/2}$ $(J=1)$	$M1$, $E2$, $M3$
$L_{1/2}L_{3/2}$	$2p_{1/2}2p_{3/2}$ $(J=1)$	$K\alpha_1$	$1s_{1/2}2p_{1/2}$ $(J=1)$	$E1$, $M2$
		$K\alpha_1$	$1s_{1/2}2p_{1/2}$ $(J=0)$	$E1$
		$K\alpha_2$	$1s_{1/2}2p_{3/2}$ $(J=2)$	$E1$, $M2$, $E3$
		$K\alpha_2$	$1s_{1/2}2p_{3/2}$ $(J=1)$	$E1$, $M2$
$L_{1/2}L_{3/2}$	$2p_{1/2}2p_{3/2}$ $(J=2)$	$K\alpha_1$	$1s_{1/2}2p_{1/2}$ $(J=1)$	$E1$, $M2$, $E3$
		$K\alpha_1$	$1s_{1/2}2p_{1/2}$ $(J=0)$	$M2$
		$K\alpha_2$	$1s_{1/2}2p_{3/2}$ $(J=2)$	$E1$, $M2$, $E3$, $M4$
		$K\alpha_2$	$1s_{1/2}2p_{3/2}$ $(J=1)$	$E1$, $M2$, $E3$
$L_{1/2}L_{3/2}$	$2s_{1/2}2p_{3/2}$ $(J=1)$	$K\alpha_1$	$1s_{1/2}2s_{1/2}$ $(J=1)$	$E1$, $M2$
		$K\alpha_1$	$1s_{1/2}2s_{1/2}$ $(J=0)$	$E1$
		$K\alpha_2$	$1s_{1/2}2p_{3/2}$ $(J=2)$	$M1$, $E2$, $M3$
		$K\alpha_2$	$1s_{1/2}2p_{3/2}$ $(J=1)$	$M1$, $E2$
$L_{3/2}L_{3/2}$	$2p_{3/2}2p_{3/2}$ $(J=2)$	$K\alpha_1$	$1s_{1/2}2p_{3/2}$ $(J=2)$	$E1$, $M2$
		$K\alpha_1$	$1s_{1/2}2p_{3/2}$ $(J=1)$	$E1$, $M2$
$L_{3/2}L_{3/2}$	$2p_{3/2}2p_{3/2}$ $(J=0)$	$K\alpha_1$	$1s_{1/2}2p_{3/2}$ $(J=2)$	$M2$
		$K\alpha_1$	$1s_{1/2}2p_{3/2}$ $(J=1)$	$E1$

sion. The degree of the anisotropy is determined both, by the initial alignment of the resonances and by the structure function of a particular transition, which includes the interference between different allowed multipole channels.

To understand how the multipole mixing influences the anisotropy parameters (6), let us consider the two $K\alpha_1$ fine-structure transitions: $2s_{1/2}2p_{3/2}(J=2) \rightarrow 1s_{1/2}2s_{1/2}(J=1)$ and $2p_{1/2}2p_{3/2}(J=1) \rightarrow 1s_{1/2}2p_{1/2}(J=1)$. For these two transitions, Fig. 1 displays the second-rank structure function from Eq. (7) for different nuclear charges Z along the helium isoelectronic sequence. While the $E1$ approximation (dotted line) always leads to a constant value [cf. expression (9)], a strong variation of the structure function is seen if the $M2$ (or even the $E3$, i.e., the electric-octupole) component is taken into account. Note, however, the different behavior of the structure function for the two transitions. For the $2s_{1/2}2p_{3/2}(J=2) \rightarrow 1s_{1/2}2s_{1/2}(J=1)$ line, the structure function increases with nuclear charge, leading to larger anisotropy, whereas it decrease in its absolute value for the $2p_{1/2}2p_{3/2}(J=1) \rightarrow 1s_{1/2}2p_{1/2}(J=1)$ transition. In the latter case, therefore, the anisotropy of the corresponding $K\alpha$ is strongly suppressed by more than a factor of 6 if, apart from the $E1$ radiation, the much weaker $M2$ decay is taken into account, cf. the right-hand panel of Fig. 1. This large effect arises mainly from the interference of the $E1$ and $M2$ multipoles, while the $M2$ contribution to the decay rate $\Gamma_{2p_{1/2}2p_{3/2}(J=1) \rightarrow 1s_{1/2}2p_{1/2}(J=1)}$ remains with less than 1% small.

Figure 1 also shows a good agreement for the structure function as obtained within two different gauges for the electron coupling to the radiation field; in the computations be-

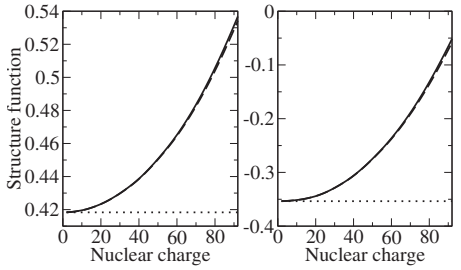

FIG. 1. Second-rank structure function $f_2(\alpha_d J_d, \alpha_f J_f)$ from Eq. (7) for the $2s_{1/2}2p_{3/2}(J=2) \rightarrow 1s_{1/2}2s_{1/2}(J=1)$ (left-hand panel) and $2p_{1/2}2p_{3/2}(J=1) \rightarrow 1s_{1/2}2p_{1/2}(J=1)$ (right-hand panel) transitions of heliumlike ions as a function of nuclear charge Z. Calculations within the electric-dipole approximation (dotted line) are compared with the full account of all of the allowed multipoles. Results from MCDF calculations are shown in Coulomb (solid line) and Babushkin gauge (dashed line).

low, we applied the Babushkin and Coulomb gauges which, within the nonrelativistic limit, are equivalent to the length and velocity form of the corresponding transition amplitudes. In the Babushkin gauge, in particular, some (multiple of a) longitudinal vector potential is added to those as obtained for the Coulomb gauge in order to test for the gauge invariance of the computations [27]. Over the whole range of nuclear charges, the structure functions f_2 differ by less than $\sim 8\%$ from each other if only transition within the singlet or triplet system of helium are considered and, for $Z \geqslant 36$, the gauge differences even become negligible for the present investigations.

A similar strong effect of the multipole mixing on the structure function and the anisotropy of the HS emission is found also for other fine-structure transitions. For example, Fig. 2 displays the f_2 functions for the $2p_{3/2}2p_{3/2}(J=2) \rightarrow 1s_{1/2}2p_{3/2}(J=1)$ and $2p_{3/2}2p_{3/2}(J=2) \rightarrow 1s_{1/2}2p_{3/2}(J=2)$ lines. For these two $K\alpha_1$ subtransitions, the shape of the angular anisotropy is quite different in the $E1$ approximation; while, for the $2p_{3/2}2p_{3/2}(J=2) \rightarrow 1s_{1/2}2p_{3/2}(J=1)$ transition, the x rays are emitted predominantly perpendicular to the ion beam, the photons leave the ion mainly parallel to the beam for the $2p_{3/2}2p_{3/2}(J=2) \rightarrow 1s_{1/2}2p_{3/2}(J=2)$ line. In this case, we have the modulus $|f_2| \approx 0.42$ for both HS lines but with a different sign for the two transitions. If the higher multipoles are included, this value for the modulus of the structure function is reduced equally to $|f_2| \approx 0.28$ due to the $M2$ contribu-

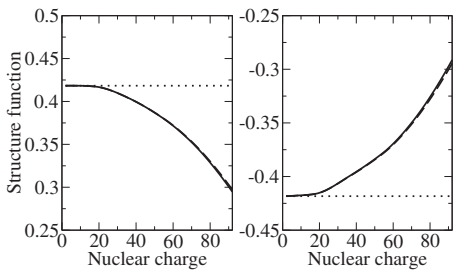

FIG. 2. The same as in Fig. 1 but for the fine-structure transitions $2p_{3/2}2p_{3/2}(J=2) \rightarrow 1s_{1/2}2p_{3/2}(J=1)$ (left-hand panel) and $2p_{3/2}2p_{3/2}(J=2) \rightarrow 1s_{1/2}2p_{3/2}(J=2)$ (right-hand panel) from the $L_{3/2}L_{3/2}$ resonance group.

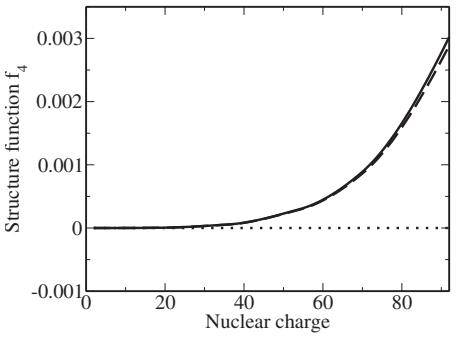

FIG. 3. Fourth-rank structure function $f_4(\alpha_d J_d, \alpha_f J_f)$ from Eq. (7) for the $2s_{1/2}2p_{3/2}(J=2) \rightarrow 1s_{1/2}2s_{1/2}(J=1)$ fine-structure transition of heliumlike ions as a function of the nuclear charge Z. Notations are the same as in Fig. 1.

tions, giving rise to a much less pronounced angular distribution of the emitted HS photons.

For the LL resonances with total angular momentum $J_d = 1$, the second-rank structure function f_2 contains all of the information about the anisotropy of a line as caused by its electronic structure. A second structure parameter f_4 is needed only for $J_d \geqslant 2$. In order to explore also the influence of the multipole mixing on the angular distribution of the $J_d=2$ decay lines, let us note that $f_4 \equiv 0$ in the $E1$ approximation as seen, for example, from the $6j$ symbol in expression (7). Therefore, a nondipole decay mode is required to have a nonvanishing f_4 value, and this fact suggests already that the fourth-rank structure function f_4 is expected to be small. This is confirmed by Fig. 3 in which this function is shown for the $2s_{1/2}2p_{3/2}(J=2) \rightarrow 1s_{1/2}2s_{1/2}(J=1)$ line. The f_4 parameter does not exceed the value 0.003 even for heliumlike uranium. In the following discussion of the $K\alpha_1$ HS, we shall therefore neglect the contribution of f_4 to the anisotropy of these lines.

So far, we have discussed the effects of the multipole mixing on the $K\alpha_1$ HS transitions for three LL resonances of heliumlike ions, namely $2s_{1/2}2p_{3/2}(J=2)$, $2p_{1/2}2p_{3/2}(J=1)$, and $2p_{3/2}2p_{3/2}(J=2)$, respectively. As seen from Table I, however, there are two other LL resonances, $2p_{1/2}2p_{3/2}(J=2)$ and $2s_{1/2}2p_{3/2}(J=1)$, which can contribute to the $K\alpha_1$ radiation and might be influenced by the multipole mixing. For these transitions, the structure functions f_2 show indeed a very similar behavior as discussed above, cf. Figs. 1 and 2 For example, the second-rank structure function f_2 from the MCDF computations for the transition $2p_{1/2}2p_{3/2}(J=2) \rightarrow 1s_{1/2}2p_{1/2}(J=1)$ agrees with that for the transition $2s_{1/2}2p_{3/2}(J=2) \rightarrow 1s_{1/2}2s_{1/2}(J=1)$ (Fig. 1, left-hand panel) within 1% for all nuclear charges. This agreement can be easily understood within the IPM model if we describe the $K\alpha_1$ HS lines simply as the $2p_{3/2} \rightarrow 1s_{1/2}$ one-electron transition, with the second electron being just a spectator in either the $2p_{1/2}$ or $2s_{1/2}$ subshell. Since the total angular momentum of the spectator electron is the same in both cases, $j_s = 1/2$, the structure function must be also identical in the IPM model according to Eq. (11). Similarly, the structure function f_2 practically coincides for the transition $2s_{1/2}2p_{3/2}(J=1) \rightarrow 1s_{1/2}2s_{1/2}(J=1)$ with that for the $2s_{1/2}2p_{3/2}(J=2) \rightarrow 1s_{1/2}2s_{1/2}(J=1)$ line (Fig. 1 right-hand panel). Moreover, a

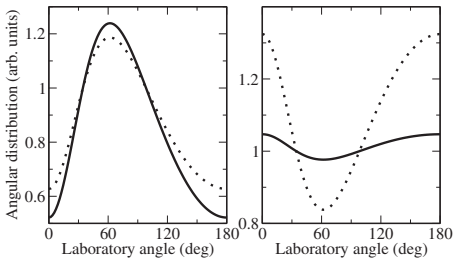

FIG. 4. Angular distribution of the $2s_{1/2}2p_{3/2}(J=2) \rightarrow 1s_{1/2}2s_{1/2}(J=1)$ (left-hand panel) and $2s_{1/2}2p_{3/2}(J=1) \rightarrow 1s_{1/2}2s_{1/2}(J=1)$ (right-hand panel) transitions of heliumlike uranium ions following the *K-LL* DR. Calculations are performed within the electric-dipole approximation (dotted line) and by taking into account all of the allowed multipoles (solid line). Results are presented in the laboratory frame.

similar analysis for the $K\alpha_2(2p_{1/2} \rightarrow 1s_{1/2})$ transitions shows that all multipoles with $L>1$ are forbidden within the IPM model. Therefore, the mixing of different multipoles are likely to be small also within the MCDF approach for all $K\alpha_2$ lines, even if these higher-order contributions are not forbidden explicitly by the selection rules for the total angular momenta of the intermediate and final states.

Apart from the structure functions f_k, the angular distribution of a given HS line depends also on the alignment of the doubly excited states as produced by the resonant electron capture. To calculate the alignment parameter $\mathcal{A}_{20}$, MCDF wave functions were applied for the initial and intermediate states, and both the static Coulomb repulsion as well as the relativistic Breit interaction were incorporated into the capture amplitudes $\langle \alpha_d J_d \| V \| \alpha_0 J_0, lj:J_d \rangle$, i.e., all computations were carried out with $V=V_{\text{Coulomb}}+V_{\text{Breit}}$. With the so obtained alignment parameters and the structure function calculated in the dipole approximation, the anisotropy parameters β_2 were found to be in very good agreement with the previous computations by Chen and Scofield [16], except for the $2p_{1/2}2p_{3/2}(J=1)$ resonance for which a factor of 4 difference was found; the reason of this discrepancy is unclear.

Figure 4 displays the angular distribution of the two HS lines $2s_{1/2}2p_{3/2}(J=2) \rightarrow 1s_{1/2}2s_{1/2}(J=1)$ (left-hand panel) and $2s_{1/2}2p_{3/2}(J=1) \rightarrow 1s_{1/2}2s_{1/2}(J=1)$ (right-hand panel) for heliumlike uranium following the DR into the hydrogenlike $U^{91+}(1s_{1/2})$ ions. Note that the angular distribution (5) is transformed from the ion frame of the projectile into the laboratory frame. For these *LL* resonances, a strong alignment of $\mathcal{A}_{20}(2s_{1/2}2p_{3/2}J=2)=-0.890$ and $\mathcal{A}_{20}(2s_{1/2}2p_{3/2}J=1)=-0.918$ was obtained. Within the *E*1 approximation (dashed lines), this results in an anisotropy of $\beta_2(2s_{1/2}2p_{3/2}J=2 \rightarrow 1s_{1/2}2s_{1/2}J=1)=-0.373$ and $\beta_2(2s_{1/2}2p_{3/2}J=1 \rightarrow 1s_{1/2}2s_{1/2}J=1)=0.324$, respectively. If higher multipoles are taken into account in the structure function, the anisotropy becomes $\beta_2(2s_{1/2}2p_{3/2}J=2 \rightarrow 1s_{1/2}2s_{1/2}J=1)=-0.479$, i.e., it increases by ~30%, while $\beta_2(2s_{1/2}2p_{3/2}J=1 \rightarrow 1s_{1/2}2s_{1/2}J=1)=0.046$ decreases even by a factor of 7. For the latter transition, we therefore expect an almost isotropic emission despite of the strong alignment of the $2s_{1/2}2p_{3/2}(J=1)$ resonance. It is obvious that such a strong change of the anisotropy due to the *M*2 and higher multipole contributions might affect also the overall emission pattern of the HS radiation.

B. Anisotropy of the $K\alpha_1$ hypersatellite radiation in U^{90+}: Comparison with experiment

A direct comparison of the calculated angular distribution with measured data is difficult to be carried out for the $K\alpha_{1,2}$ (fine-structure) HS lines because of several experimental restrictions. In present-day collision experiments of relativistic projectiles with gas-jet targets, difficulties may arise especially from uncertainties in the energy (profile) of the ion beam, the still rather low resolution in the angle-resolved x-ray detection as well as from statistics. In the measurements by Ma and co-workers [12], therefore only three rather broad peaks were observed for the $K\alpha_1$, and similarly for the $K\alpha_2$, HS radiation, and these peaks were assigned to the emission from the $L_{1/2}L_{1/2}$, $L_{1/2}L_{3/2}$, and the $L_{3/2}L_{3/2}$ groups of resonances (cf. Table I). The (relative) population of the individual resonances within these groups remained unclear, in contrast, because of the incomplete knowledge of the velocity distribution of the ions, the Compton profile (momentum distribution) of the target electrons as well as the width of the individual resonances (that differs by about a factor 2 between 30 and 60 eV). In the computations, therefore, only an equal electron distribution can be assumed at best for all the resonances of a given group, e.g., by simply choosing the initial population of the resonances due to their capture probabilities (3).

For the further analysis of the $K\alpha$ angular distribution, we restrict ourselves to the x-ray emission that arises from the four $L_{1/2}L_{3/2}$ resonances with $J=1,2$. For each of these resonances, there occur several fine-structure transitions to different $1s_{1/2}2ljJ_f$ final states of the HS emission, and these transitions have been summed incoherently by using the calculated branching ratios. Such an incoherent summation neglects possible interferences between neighbored resonances but these effects are expected to be small for heliumlike uranium. For the four resonances of the $L_{1/2}L_{3/2}$ group, Fig. 5 displays the calculated $K\alpha_1/K\alpha_2$ intensity ratio for U^{90+} ions. Again, two approximations are shown for only the *E*1 radiation (dotted lines) as well as with full account of all allowed multipoles (solid lines). As seen from this figure, the multipole mixing leads to an enhancement of the $K\alpha_1/K\alpha_2$ ratio by about 30% in all four cases. For the radiative decay of the $2p_{1/2}2p_{3/2}(J=2)$ level, for example, the anisotropy parameter increases from $\beta_2=-0.499$ in the *E*1 approximation to almost $\beta_2=-0.637$, if the higher multipoles are taken into account.

As argued above, a further assumption concerning the (initial) population of the individual resonances need to be made in order to compare the $K\alpha_1/K\alpha_2$ intensity ratio with previous computations and experiment. In the following, here we simply apply the theoretical DR capture rates (i.e., a constant probability distribution for the electrons which is spread over all resonances of interest) in order to define their relative population. In Fig. 6, the angular distribution of the $K\alpha_1/K\alpha_2$ ration is shown, averaged over the four resonances, and compared with the measurements by Ma *et al.* [12]. A very strong anisotropy of about −0.75 was found in the experiment which is not reproduced by our theory, even if higher multipoles are taken into account. Nevertheless, a clear enhancement of the anisotropy is obtained for this ratio

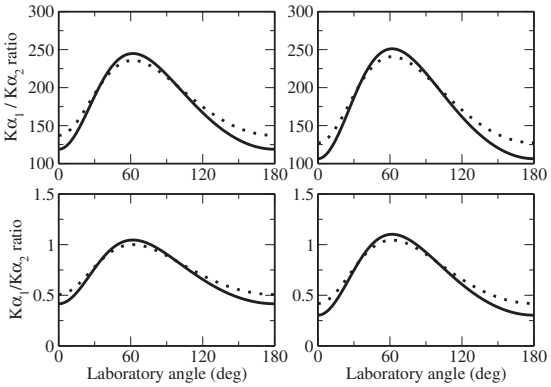

FIG. 5. Intensity ratio of the $K\alpha_1/K\alpha_2$ HS lines for heliumlike uranium following the DR into the $L_{1/2}L_{3/2}$ resonances. Calculations are performed within the $E1$ approximation (dotted line) and by taking into account all of the allowed multipoles (solid line). Top-left-hand panel: $2s_{1/2}2p_{3/2}(J=1)$ with $\beta_2^{(E1)}(K\alpha_1)=-0.324$ in the $E1$ approximation and $\beta_2(K\alpha_1)=-0.414$ with full account of all multipoles. Top-right-hand panel: $2s_{1/2}2p_{3/2}(J=2)$ with $\beta_2^{(E1)}(K\alpha_1)=-0.373$ and $\beta_2(K\alpha_1)=-0.476$. Bottom-left-hand panel: $2p_{1/2}2p_{3/2}(J=1)$ with $\beta_2^{(E1)}(K\alpha_1)=-0.393$ and $\beta_2(K\alpha_1)=-0.502$. Bottom-right-hand panel $2p_{1/2}2p_{3/2}(J=2)$ with $\beta_2^{(E1)}(K\alpha_1)=-0.499$ and $\beta_2(K\alpha_1)=-0.637$. For the $K\alpha_2$ transitions, the β_2 value is negligible in all cases.

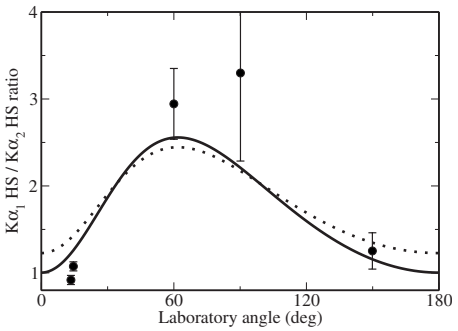

FIG. 6. Intensity ratio of the $K\alpha_1/K\alpha_2$ HS lines for heliumlike uranium following the DR at a projectile energy of $T_p=125$ MeV/u. Calculations are performed within the $E1$ approximation (dotted line) and by taking into account all of the allowed multipoles (solid line).

from $\beta_2^{\text{eff}}(K\alpha_1)=-0.398$ in the $E1$ approximation to -0.509 with the full account of all multipoles. The $E1$ value also compares well with the previous computations by Zakowicz an co-workers [19] who obtained $\beta_2^{\text{eff}}(K\alpha_1)=-0.384$ in the same approximation. While the experimental value could nearly be obtained for a predominant population of the $2p_{1/2}2p_{3/2}(J=2)$ resonance, the largest possible value in the $E1$ approximation is just -0.499.

V. SUMMARY AND OUTLOOK

We have investigated the $K\alpha$ HS radiation of high-Z heliumlike ions following the DR of hydrogenlike projectiles. In this study, emphasis was placed on the alignment of the doubly excited ions and on the effects of the higher multipoles on the angular distribution of the subsequent $K\alpha$ emission. Within the density matrix theory, the anisotropy of a given line is determined by the product of the alignment of the intermediate LL resonances with a structure function that purely depends on the electronic properties of the ions and that includes the multipole mixing. Computations are performed for the DR of initially hydrogenlike uranium with the subsequent emission of the $K\alpha$ HS lines. We have shown that the interference between the multipole components can either decrease or enhance the anisotropy of individual fine-structure transitions, and that this effect can be as large as a factor of 6. A quite sizeable change occurs also for the effective anisotropy of the $K\alpha_1/K\alpha_2$ ratio (when averaged over all four resonances from the $L_{1/2}L_{3/2}$ group) which increases by about 30%, in good agreement with experiment. Experiments with higher resolution in the x-ray spectra and with the excitation of just one of the K-LL resonances would therefore be desirable in order to understand better the effects of higher multipoles and relativity on the (DR) population and decay mechanisms of high-Z ions.

ACKNOWLEDGMENTS

S.F. acknowledges the support by DFG (Contract No. FR 1251/13-1) and GSI under Contract No. KS-FRT. N.M.K. acknowledges the hospitality and financial support from GSI. A.S. acknowledges support from the Helmholtz Gemeinschaft (Nachwuchsgruppe VH-NG-421).

[1] D. R. Bates, Case Stud. At. Phys. **4**, 62 (1974).
[2] J. Dubau and S. Volonté, Rep. Prog. Phys. **43**, 199 (1980).
[3] Y. Hahn, Adv. At. Mol. Phys. **21**, 123 (1985).
[4] P. Beiersdorfer, T. W. Phillips, K. L. Wong, R. E. Marrs, and D. A. Vogel, Phys. Rev. A **46**, 3812 (1992).
[5] K. Kollmar, P. Grün, and W. Scheid, Eur. Phys. J. D **10**, 27 (2000).
[6] W. Shi, T. Bartsch, C. Böhme, C. Brandau, A. Hoffknecht, H. Knopp, S. Schippers, A. Muller, C. Kozhuharov, K. Beckert, F. Bosch, B. Franzke, P. H. Mokler, F. Nolden, M. Steck, T. Stöhlker, and Z. Stachura, Phys. Rev. A **66**, 022718 (2002).
[7] A. Müller, Adv. At., Mol., Opt. Phys. **55**, 293 (2008).
[8] S. Schippers, A. Müller, G. Gwinner, J. Linkemann, A. A. Saghiri, and A. Wolf, Astrophys. J. **555**, 1027 (2002).
[9] E. W. Schmidt, D. Bernhardt, A. Müller, S. Schippers, S. Fritzsche, J. Hoffmann, A. S. Jaroshevich, C. Krantz, M. Lestinsky, D. A. Orlov, A. Wolf, D. Lukic, and D. W. Savin, Phys. Rev. A **76**, 032717 (2007).
[10] T. Kandler, P. H. Mokler, T. Stöhlker, H. Geissel, H. Irnich, C. Kozhuharov, A. Kriessbach, M. Kucharski, G. Münzenberg, F. Nickel, P. Rymuza, C. Scheidenberger, Z. Stachura, T. Suzuki, A. Warczak, D. Duavergne, and R. W. Dunford, Phys. Lett. A **204**, 274 (1995).
[11] P. H. Mokler, T. Kandler, T. Stöhlker, H. Geissel, C. Kozhu-

harov, P. Rymuza, C. Scheidenberger, Z. Stachura, A. Warczak, and R. W. Dunford, Phys. Scr., T **73**, 247 (1997).
[12] X. Ma, P. H. Mokler, F. Bosch, A. Gumberidze, C. Kozhuharov, D. Liesen, D. Sierpowski, Z. Stachura, Th. Stöhlker, and A. Warczak, Phys. Rev. A **68**, 042712 (2003).
[13] T. Stöhlker, D. Banas, S. Fritzsche, A. Gumberidze, C. Kozhuharov, X. Ma, A. Orsic-Muthig, U. Spillmann, D. Sierpowski, A. Surzhykov, S. Tachenov, and A. Warczak, Phys. Scr., T **110**, 384 (2004).
[14] S. Fritzsche, P. Indelicato, and T. Stöhlker, J. Phys. B **38**, S707 (2005).
[15] M. Gail, N. Grün, and W. Scheid, J. Phys. B **31**, 4645 (1998).
[16] M. H. Chen and J. H. Scofield, Phys. Rev. A **52**, 2057 (1995).
[17] N. M. Kabachnik, S. Fritzsche, A. N. Grum-Grzhimailo, M. Meyer, and K. Ueda, Phys. Rep. **451**, 155 (2007).
[18] Although the notation of the $K\alpha$ (hyper) satellite photons is a bit confusing, it occurs frequently in the literature and has been adopted here also for the heliumlike ions; historically, the $K\alpha$, satellites refer to transitions with additional vacancies in the L shell, and the hypersatellites to those with an initially empty K shell.
[19] S. Zakowicz, Z. Harman, N. Grün, and W. Scheid, Phys. Rev. A **68**, 042711 (2003).
[20] S. Zakowicz, W. Scheid, and N. Grün, Nucl. Instrum. Methods Phys. Res. B **205**, 386 (2003).
[21] A. Surzhykov, S. Fritzsche, A. Gumberidze, and Th. Stöhlker, Phys. Rev. Lett. **88**, 153001 (2002).
[22] V. V. Balashov, I. V. Bodrenko, V. K. Dolinov, and S. I. Strakhova, Opt. Spectrosc. **77**, 801 (1994).
[23] K. Blum, *Density Matrix Theory and Applications*, 2nd ed. (Plenum, New York, 1996).
[24] V. V. Balashov, A. N. Grum-Grzhimailo, and N. M. Kabachnik, *Polarization and Correlation Phenomena in Atomic Collisions* (Kluwer Academic, Plenum, New York, 2000).
[25] E. G. Berezhko and N. M. Kabachnik, J. Phys. B **10**, 2467 (1977).
[26] A. Surzhykov, U. D. Jentschura, Th. Stöhlker, and S. Fritzsche, Phys. Rev. A **73**, 032716 (2006).
[27] I. P. Grant, J. Phys. B **7**, 1458 (1974).
[28] S. Fritzsche, A. Surzhykov, and T. Stöhlker, Phys. Rev. A **72**, 012704 (2005).
[29] S. Fritzsche, C. Froese Fischer, and C. Z. Dong, Comput. Phys. Commun. **124**, 340 (2000).
[30] S. Fritzsche, H. Aksela, C. Z. Dong, S. Heinäsmäki, and J. E. Sienkiewicz, Nucl. Instrum. Methods Phys. Res. B **205**, 93 (2003).
[31] I. P. Grant, Adv. Phys. **19**, 747 (1970).
[32] I. P. Grant, in *Methods in Computational Chemistry*, edited by S. Wilson (Plenum, New York, 1988), Vol. 2, p. 1.
[33] S. Fritzsche, J. Electron Spectrosc. Relat. Phenom. **114–16**, 1155 (2001); S. Fritzsche, Phys. Scr., T **T100**, 37 (2002).
[34] F. A. Parpia, C. Froese Fischer, and I. P. Grant, Comput. Phys. Commun. **94**, 249 (1996).
[35] S. Fritzsche, C. Froese Fischer, and G. Gaigalas, Comput. Phys. Commun. **148**, 103 (2002).
[36] G. Gaigalas, S. Fritzsche, and I. P. Grant, Comput. Phys. Commun. **139**, 263 (2001).
[37] S. Fritzsche, J. Nikkinen, S.-M. Huttula, H. Aksela, M. Huttula, and S. Aksela, Phys. Rev. A **75**, 012501 (2007).
[38] G. Gaigalas, T. Zalandauskas, and S. Fritzsche, Comput. Phys. Commun. **157**, 239 (2004).
[39] S. Fritzsche, G. Zschornack, G. Musiol, and G. Soff, Phys. Rev. A **44**, 388 (1991).
[40] R. Cowan, *The Theory of Atomic Structure and Spectra* (University of California Press, Berkley, 1981).
[41] I. I. Sobel'man, *Introduction to the Theory of Atomic Spectra* (Pergamon, Oxford, 1972).
[42] A. Surzhykov, P. Koval, and S. Fritzsche, Comput. Phys. Commun. **165**, 139 (2005).